# Delayed and quasi-synchronous response of tropical Atlantic surface salinity to rainfall.

Semyon A. Grodsky[1] and James A. Carton[1]
December 4, 2017

Key points:

(1) Rainfall-induced tropical Atlantic SSS combines quasi-instantaneous response to open ocean rainfall and delayed response to river discharge

(2) ENSO-induced and Atlantic meridional mode-induced rainfall produce different delay in the Amazon discharge

(3) Persistence of anomalous SSS in the Amazon plume is limited by the seasonal wind acceleration in boreal winter

[1]Department of Atmospheric and Oceanic Science, University of Maryland, College Park

Corresponding author: senya@umd.edu

**Abstract**

River discharge impact on sea surface salinity (SSS) is particularly evident in the western tropical Atlantic where the Amazon and Orinoco represent two out of the four largest discharges. This continental discharge is fed by tropical rainfall, which variability is dominated by meridional (dipole) and ENSO-induced modes that are partitioned between ocean and land. Such partitioning implies a complex ocean response. While SSS response to local ocean rainfall is almost instantaneous, its response to land rainfall is delayed by riverine hydrology. Land rainfall associated with the meridional rainfall mode concentrates mostly over the coastal north-east Brazil and results in a fast Amazon response. In contrast, ENSO-induced rainfall anomaly occupies vast inland areas and leads to Amazon discharge response delayed by 3 to 7 months. Although ocean profile analyses represent well interannual SSS forced by open ocean rainfall, they don't resolve well interannual SSS in the plume, which is better represented by ocean reanalyses. In Simple Ocean Data Assimilation, the plume anomaly persists several months following the peak of rainfall and is diffused by seasonally accelerating winds in boreal winter. But, its magnitude is a modest few tenth of PSU and only marginally statistically significant. Perhaps, such weak correlation of SSS and continental discharge variations is not surprising due to other factors contributing in this dynamically active area. Significant transient variability not associated with ocean and land rainfall is a factor explaining why profile analyses don't resolve interannual variability of the Amazon plume.

## 1. Introduction

A striking feature of the Atlantic Ocean is the appearance of salty pools (>37psu) in the subtropics due to high evaporation and lack of rainfall. These subtropical sea surface salinity

(SSS) maxima are separated from lower SSS in the rainy tropics (Dessier and Donguy, 1994), where SSS is diluted by local ocean rainfall and by rainfall over adjacent land discharged by tropical rivers. Here we use SSS observations to describe that such rainfall partitioning implies a complex SSS response. While SSS response to ocean rainfall is almost instantaneous, its response to land rainfall is delayed by the continental hydrology (Chen et al., 2010).

The seasonal mixed layer salt storage in the tropical Atlantic is controlled by several seasonally varying processes (Foltz et al., 2004), among which the high precipitation under the Intertropical Convergence Zone (ITCZ) and the discharge of major tropical rivers are both important (e.g. Lentz, 1995). Between 10°S-15ºN SSS is diluted by the seasonally migrating ITCZ and its southern counterpart (Grodsky and Carton, 2003). This fresh SSS is advected both zonally (by the seasonally developing North Equatorial Counter Current, NECC, e.g. Carton and Katz, 1990) and meridionally (through Ekman transport by the trade winds, e.g. Grodsky et al., 2014b; Foltz et al., 2015). West of 40ºW mixed layer salinity is significantly freshened by the Amazon, whose discharge peaks in mid-May and decreases to its seasonal minimum in mid-November, reflecting the seasonal march of the ITCZ and water storage processes over the catchment area (Lentz, 1995). By early boreal fall the Amazon water spreads over a $10^6$ $km^2$ fresh pool west of 40ºW (Dessier and Donguy, 1994), producing a large area with near-surface barrier layers (e.g. Liu et al., 2009) capable of affecting local air-sea interactions, even under hurricane winds (e.g. Grodsky et al., 2012).

Besides the seasonal variability, tropical Atlantic rainfall and related river discharge vary interannually. The leading mode of interannual rainfall variability peaks in spring and is associated with the tropical Atlantic interhemispheric sea surface temperature (SST) difference that governs anomalous meridional atmospheric pressure difference and related shifts of the ITCZ, which in turn affect rainfall and storage redistribution among northern and southern tributaries of the Amazon (Hastenrath and Heller, 1977; Nobre and Shukla, 1996; Chiang et al., 2002). Variations in the Amazon rainfall are related to the effect of tropical Atlantic SST on the Hadley cell and the corresponding subsidence over the Amazon. This variability peaks in the March-May season immediately preceding the peak of Amazon discharge (e.g. Espinoza et al., 2009). The strongest recent interannual event is related to the 2009 anomalous cooling of tropical North Atlantic SST and related southward shifts of the ITCZ (Foltz et al., 2012). Besides interannual events, the interhemispheric mode also experiences decade-scale oscillations driven by the wind-evaporation-SST feedback (Xie and Carton, 2004). The strength of Atlantic SST influence on the Amazon is comparable in magnitude to Pacific SST influence (Yoon and Zeng, 2010).

Besides the interhemispheric mode, the tropical Atlantic rainfall also experiences El-Nino Southern Oscillations (ENSO) induced variations (Kousky et al., 1984) that extend in a spatially coherent pattern over the tropical South America and Atlantic (Ropelewski and Halpert, 1987; Chiang et al., 2002). Interannual Amazon rainfall induced by changes in Pacific SST peaks in the November–March season and leads the seasonal Amazon discharge peak (May – June) by several months (Espinoza et al., 2016). The origin of the ENSO impact is linked to Pacific SST effect on the atmospheric Walker Cell (Gill, 1980; see also Sasaki et al., 2015 and references therein). During El Niño, an enhanced convection over warm eastern equatorial Pacific is accompanied by corresponding enhancement of downstream atmospheric descent over the

Atlantic sector, which in turn caps local convection and decreases rainfall. The two rainfall modes are not completely independent because tropical Pacific SST influences the north tropical Atlantic through atmospheric teleconnections and thus affects the meridional SST gradient in the tropical Atlantic that shifts the ITCZ (Nobre and Shukla, 1996, Enfield and Mayer, 1997).

As evidenced above, Pacific and Atlantic SST may affect the sea surface salinity (SSS) in the Amazon plume via its influences on the Amazon rainfall and discharge. Through EOF decomposition of ocean data assimilation simulations, Tyaquiçã et al. (2017) have shown that the leading mode of anomalous SSS in the Amazon plume presents an ENSO-induced response that lags behind the Amazon rainfall by ~3 months. Although ENSO-induced variations explain about 50% of observed SSS variability in the Amazon plume (Zeng et al., 2008), other factors contribute as well. They include cross-shore winds that modify offshore freshwater dispersal (Molleri et al., 2010) and appear to be related to the tropical Atlantic meridional SST mode (Fournier et al., 2017). It is also probable that interannual variability in regional surface currents not associated with local winds (Grodsky et al., 2014a) may account for the remaining portion of interannual SSS variability.

Interannual rainfall in the tropical Atlantic is dominated by the two leading modes that extend over adjacent land and have differing impacts on variations of the Amazon discharge. This paper explores if observed SSS allows for distinguishing between impacts of the two rainfall modes as well as between the delayed SSS response to Amazon discharge and the quasi-instantaneous response to ocean rainfall.

## 2. Data and Methods

Ocean rainfall, evaporation, SST, and winds are characterized using the Era-Interim reanalysis of atmospheric parameters produced by the ECMWF (Dee et al., 2011). The ERA-Interim data used in this study are monthly averages on a 1° regular grid available at ( https://www.ecmwf.int/en/research/climate-reanalysis/reanalysis-datasets/era-interim ) . Monthly land rainfall is characterized by the Global Precipitation Climatology Project (GPCP v.2.3, e.g. Adler et al., 2003) combined gauge/satellite rainfall analysis (http://eagle1.umd.edu/GPCP_ICDR/GPCPmonthlyV2.3.pdf ) available on a regular 2.5° grid at (http://gpcp.umd.edu/ ).

For near surface salinity data, two 'Argo+' data-only analyses available through (http://www.argo.ucsd.edu/Gridded_fields.html) are examined. The Japan Agency for Marine-Earth Science and Technology (JAMSTEC) employs 2-dimensional optimal interpolation of Argo floats, ocean mooring data, and CTD casts on pressure surfaces for monthly analysis of temperature and salinity on a global 1°x1° grid from January 2001-ongoing (Hosoda et al., 2008). The Scripps Institute of Oceanography analysis (SCRIPPS) is based only on Argo data. By decomposing data into climatology and monthly anomaly fields, this analysis is able to resolve finer spatial scales for monthly analysis on a global 1°x1° grid from January 2004-ongoing (Roemmich and Gilson, 2009). As a proxy for SSS, the shallowest level salinity is used for each analysis, from which anomalies are calculated by subtracting the corresponding monthly seasonal cycle.

Although the two analyses resolve low SSS in the Amazon plume, it appears that its interannual variability is not resolved well. For a better representation of high variable Amazon plume SSS, the Simple Ocean Data Assimilation (SODA version 3) is used. Particular run used in this study (SODA 3.4.2, http://www.atmos.umd.edu/~ocean/index_files/soda3.4.2_mn_download.htm ) is driven by Era-Interim surface forcing and monthly river discharge (Dai et al., 2009) spans 1980-2015.

Observed monthly discharge at Obidos station is used as a simple proxy for Amazon discharge. It is compared to the combined Amazon–Tocantins River discharge evaluated as a sum of discharges of the Amazon (at Obidos), Tapajos, Xingu, and Tocantins. The Amazon discharge, its main southern tributary discharges, as well as the Orinoco discharge (since 2003) are available at (http://www.ore-hybam.org ). For the earlier period, the Dai (2016) Orinoco discharge is used (https://doi.org/10.5065/D6V69H1T ). The downstream Tocantins discharge at Tucurui is available from the Brazil's national grid operator website (http://www.ons.org.br/Paginas/resultados-da-operacao/historico-da-operacao/dados_hidrologicos_vazoes.aspx ).

Pacific and Atlantic SST is characterized by the NINO3 and the Atlantic Meridional Mode (AMM, Chiang and Vimont, 2004) indices available at https://www.esrl.noaa.gov/psd/gcos_wgsp/Timeseries/Nino3/ and https://www.esrl.noaa.gov/psd/data/timeseries/monthly/AMM/ammsst.data, respectively.

Satellite SSS is monthly Level 3 Aquarius version 5.0 SSS (August 2011 through June 2015) obtained from the NASA Goddard Space Flight Center on a 1°x1° grid (https://oceandata.sci.gsfc.nasa.gov/Aquarius/Mapped/Monthly/1deg/V5.0_SSS/ ). It has a characteristic accuracy of 0.2 psu for monthly averages (see Lee, 2016 for more detailed accuracy analysis). The Soil Moisture Active Passive (SMAP) salinity mission that followed the AQUARIUS salinity mission began salinity observations in late March, 2015. Monthly 0.25°x0.25° SMAP (version 2) SSS used in this paper is distributed by the Remote Sensing Systems (Meissner and Wentz, 2016) and available at ftp://ftp.remss.com/smap/SSS/L3/V02.0 .

## 3. Results

### *3.1 Anomalous rainfall variability modes*

The surface flux component affecting ocean mixed layer salinity is the surface freshwater flux, $(P - E) * S$, that is proportional to the precipitation -minus-evaporation difference, PmE. In the tropical Atlantic, the variability of anomalous PmE is dominated by the two leading zonally elongated modes (Figure 1a). Both modes are dominated by precipitation (with evaporation playing a secondary role) and are repeatedly referred as simply rainfall modes.

The first EOF reflects a dipole rainfall pattern resulting from meridional shifts of the ITCZ forced by the interhemispheric SST difference in the tropical Atlantic (Nobre and Shukla, 1996). The correspondence between this rainfall mode and the tropical Atlantic SST is illustrated by the correlation map (Figure 1a) and by almost in-phase (to within 1 month) lagged correlation of the first rainfall mode principal component time series (PC1) with the AMM index (Figure 2a). The strongest 'negative' interannual event in the first rainfall mode (Figure 1c) is associated with the

2009 anomalous cooling of the tropical North Atlantic SST and corresponding southward shift of the ITCZ (Foltz et al., 2012). This mode is also coincident with trade winds acceleration/deceleration over cold/warm SST, respectively (Figure 1a, Xie and Carton, 2004). Noticeably, the meridional wind pattern is responsible for stronger/weaker onshore component of the northeasterly trade winds along the coast of northeastern South America during cold/warm north tropical Atlantic SST events, respectively. As has shown by Molleri et al. (2010) and Fournier et al. (2017), the strength of onshore wind component impacts spatial dispersion and areal extent of the Amazon/Orinoco plume.

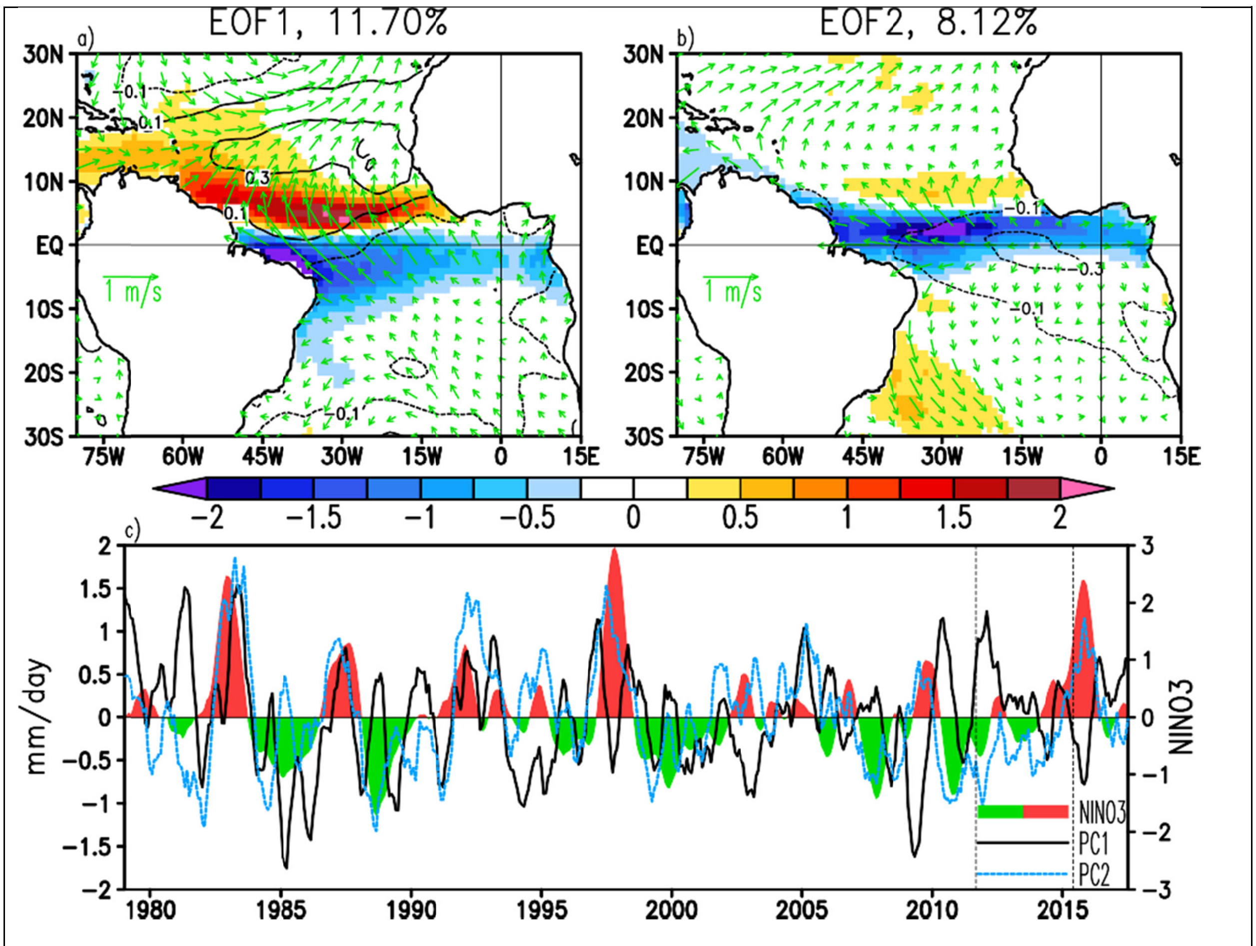


**Figure 1**. (a,b) Spatial (EOF) and (c) temporal (PC) parts of the two leading EOFs of anomalous monthly ERA-I rainfall-minus-evaporation. Corresponding PC regression with anomalous SST (contours, degC) and 10m wind (arrows) are also shown in (a) and (b). NINO3 index is shown in (c). All time series are ±3 month smoothed. Vertical lines in (c) mark the AQUARIUS period

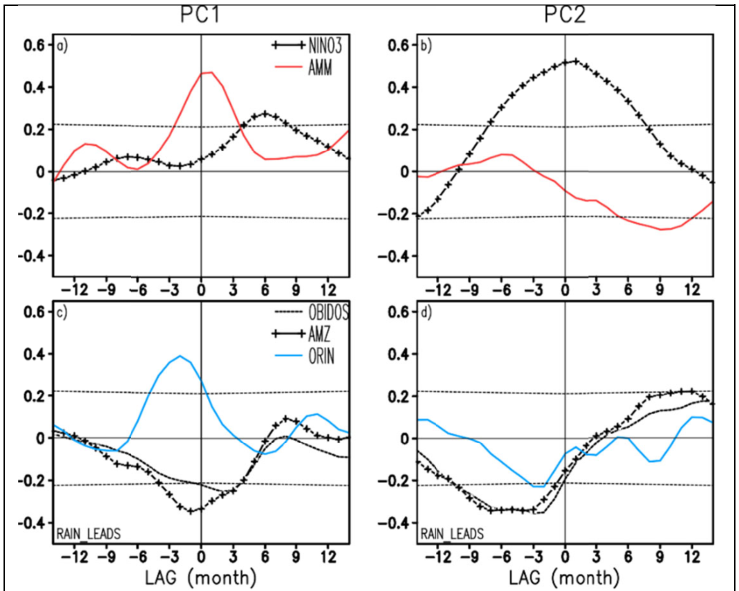


**Figure 2**. Lagged correlation of ocean rainfall principal components (from Figure 1c) with (a, b) NINO3 and Atlantic Meridional Mode (AMM) indices, (c, d) anomalous monthly Amazon volume transport at Obidos, combined Amazon transport (Obidos, Xingu, Tapajos, and Tocantins, AMZ), and Orinoco transport (ORIN). The 99% confidence intervals of zero correlation are shown by thin dashed lines.

The second rainfall EOF (Figure 1b) also extends across the tropical Atlantic, but in distinction from the first (dipole-like) mode, it doesn’t change sign and reflects an in-phase ENSO-induced response of tropical South America and tropical Atlantic rainfall (Ropelewski and Halpert, 1987). The close association between time series of PC2 and NINO3 (Figure 1c) arises in part due to the ENSO effect on the Walker circulation. During El Niño, an enhanced Pacific convection strengthens the Walker Cell and increases tropospheric warming. Downstream over the Atlantic sector, these Pacific influences are accompanied by enhanced atmospheric subsidence (e.g. Kousky et al., 1984) and increased vertical stability of the atmospheric column (Chiang et al., 2002), both of which depress local convection and rainfall. This rather fast atmospheric teleconnections lead to almost in-phase rainfall response over the Atlantic sector (Figure 2b). The width of lagged correlation between time series of PC2 and NINO3 apparently exceeds that for the meridional mode (Figure 2a) and reflects a wide spectrum of atmospheric mechanisms involved in Pacific SST teleconnections, including local tropical impacts on the Walker cell as well as mid-latitude blocking in the southeastern Pacific in combination with an intense subtropical jet (e.g. Ronchail et al., 2002).

In distinction from the EOF decomposition, real rainfall modes are not completely independent because ENSO-induced Pacific SST influences atmospheric circulation and SST over the northern tropical Atlantic through atmospheric teleconnections into higher latitudes of the Northern Hemisphere and thus affects the meridional SST pattern and shifts the ITCZ (Enfield and Mayer, 1997). This ENSO - north tropical Atlantic SST teleconnection is reflected in a remaining weak PC1 & NINO3 correlation that lags behind the NINO3 by about 6 months (Figure 2a).

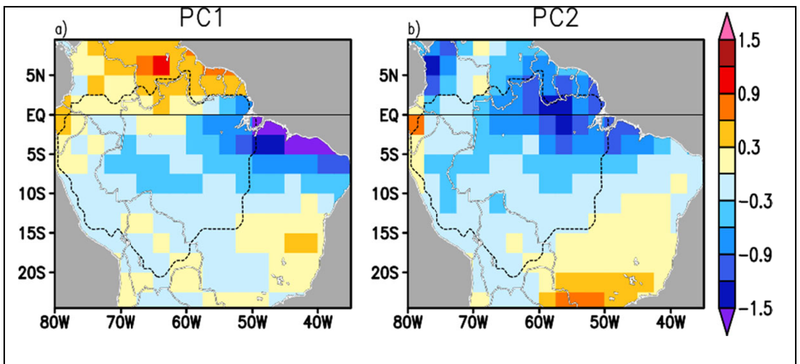


**Figure 3**. Temporal regression of ocean rainfall principal components (Figure 1c) on GPCP land rainfall (mm/dy) for (a) meridional rainfall mode (PC1) and (b) ENSO rainfall mode (PC2). Amazon catchment area is shown by dashed.

Zonal patterns of rainfall EOFs (Figure 1a,b) extend over South America and account for AMM-induced and ENSO-induced rainfall variability over the Amazon catchment area (Figure 3). Perhaps such variability is not surprising since rainfall over the continent has often been linked to variations in Pacific and Atlantic SSTs (e.g. Ropelewski and Halpert, 1987; Nobre and Shukla, 1996; Chiang et al., 2002; Yoon and Zeng, 2010). In particular, the Amazon discharge undergoes interannual and decadal changes including a 10% higher discharge during La Niña (e.g. Amarasekera et al., 1997). Spatial patters associated with ENSO- and AMM-induced rainfall are different. ENSO-induced rainfall pattern (Figure 3a) occupies vast inland areas extending into the middle Amazon. Due to water storage, this extended pattern causes a phase delay in the corresponding rainfall–discharge relationship (Chen et al., 2010). The bottom of lagged correlation between the anomalous Amazon discharge and the NINO3 has rather wide shape. It reflects weaker rainfall caused by warmer Pacific SST that results in anomalous Amazon discharge lagging behind the NINO3 by 3 to 7 months (Figure 2d). Because of the spatially large pattern of anomalous rainfall (Figure 3a), most of the Amazon discharge anomaly is accounted for by Obidos volume transport while the inclusion of southern tributaries plays a minor role (Figure 2d).

In contrast to ENSO-induced rainfall pattern, AMM-induced dipole rainfall pattern concentrates over coastal northeastern South America (Figure 3b) implying a shorter transport time to river mouths and thus a smaller rainfall-discharge delay. It also implies a stronger relative contribution of southern tributaries of the Amazon and the Tocantins River. For the meridional rainfall mode, the combined Amazon discharge displays only a minor (~ 1month) lag behind rainfall PC1. The inclusion of anomalous discharge produced by southern tributaries of the Amazon increases the magnitude of rainfall-discharge correlation (Figure 2c). This is in contrast with ENSO-induced Amazon discharge variability for which tributaries have a little impact (Figure 2d). Note also that AMM-induced Amazon and Orinoco discharge variations are out of phase (Figure 2c) in line with the meridional dipole pattern (Figure 3a).

*3.1 SSS response to anomalous rainfall*

Next, we will examine tropical Atlantic SSS response to the leading rainfall modes. A complex SSS response is anticipated due to the combination of freshwater forcing from ocean rainfall and land rainfall. This is further complicated by the multimode rainfall variability and the difference in lagged response of the Amazon River to particular rainfall mode.

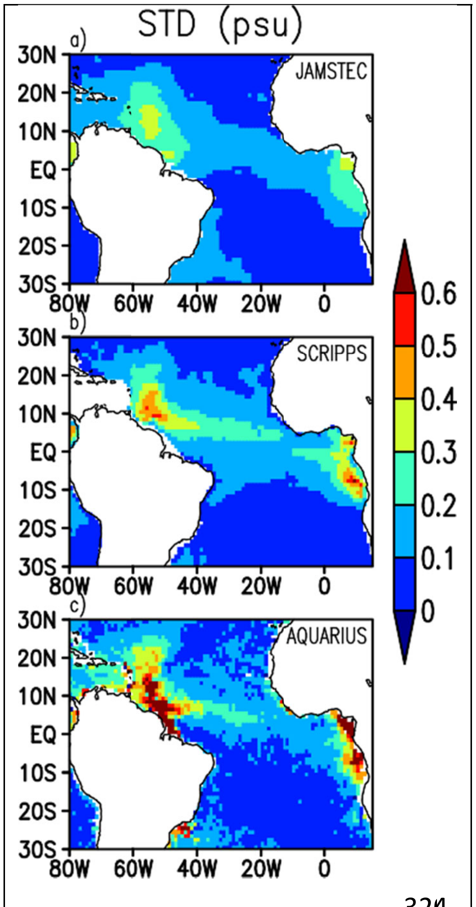


**Figure 4.** Standard deviation (STD) of monthly SSS anomaly from in-situ profile analyses (a) JAMSTEC, (b) SCRIPPS, and (c) AQUARIUS satellite.

**In situ salinity** Resolving interannual periods associated with either the ENSO or AMM requires rather long time series. For these, we focus on ocean profile analyses spanning the Argo period (JAMSTEC and SCRIPPS). The spatial pattern of the magnitude of non-seasonal SSS resembles the pattern of Amazon plume export pathways (e.g. Grodsky et al., 2014a) with maxima along directional lobes extending into the north subtropical Atlantic (northeast of the Lesser Antilles) and the central tropical Atlantic along the North Equatorial Countercurrent (NECC, Figure 4). The third, Caribbean pathway is not represented well because of weak Argo coverage (the SCRIPPS analysis is just blanked there). Depending on the particular analysis, the magnitude of SSS variability varies significantly (compare Figures 4a, b) that is explained by different objective interpolation techniques (stronger smoothing in the JAMSTEC). The magnitude of variability of near-surface salinity deducted from the SCRIPPS analysis is closer to that based on the AQUARIUS observations, but its magnitude in the Amazon plume is still weaker (Figure 4). This suggests that at least a portion of SSS variability in the plume is not resolved by either of in-situ profile analyses. It appears that not only a portion of SSS variance is not represented, but the temporal variations are not resolved satisfactorily by in-situ profile analyses. As we will further see, the latter leads to a lack of correlation between rainfall principal components and analyzed plume salinity.

In contrast to the Amazon plume SSS, the open ocean SSS variability is resolved well by either of profile analyses (Figure 5). Its patterns describe deviations from the time mean SSS, which has a well-known local minimum in the ITCZ latitude band, but is slightly displaced northward with respect to the PmE minimum latitude due to the Ekman advection (e.g. Yu et al., 2015).

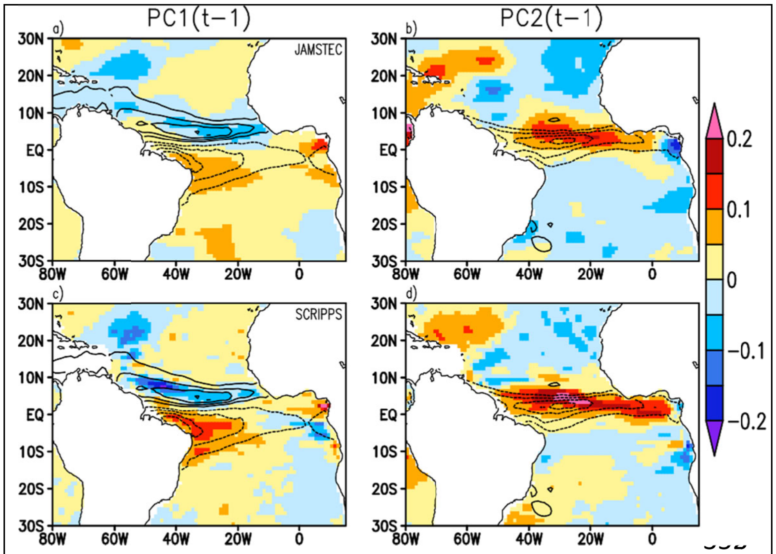


**Figure 5**. Temporal regression of ocean rainfall principal components (from Figure 1c) with monthly anomalous SSS from (a,b) JAMSTEC, (c, d) SCRIPPS. Color scale is in (psu/$PC_{unit}$). Regression maps correspond to PC1 and PC2 leading SSS by 1 month. Spatial rainfall EOFs (Figure 1a, b) are overlain as contours.

Spatial patterns of the temporal regression of anomalous SSS with principal components of the two leading rainfall modes are consistent for the two analyses (Figure 5). They depict an expected SSS response that maximizes quasi-instantaneously with rainfall (a minor 1 month lag is present) and closely correspond to spatial patterns of the surface freshwater forcing (Figure 5). The meridional rainfall mode produces a dipole-like SSS pattern. In particular, northward shifts of the ITCZ decrease SSS in the 5N-10N corridor and increases SSS off the eastern tip of South America (Figures 5 a, c). The magnitude of SSS variations is stronger for the SCRIPPS (~0.15 psu/$PC_{unit}$, Figure 5c) suggesting up to 0.5 psu interannual magnitude (see Figure 1c for the magnitude of PC1 variations). Meridional shifts of ocean rainfall are accompanied by corresponding shifts of the Amazon rainfall (Figure 3a), which predominantly occupy the lower Amazon basin and lead to almost in-phase changes of the Amazon discharge (Figure 2c). Although such discharge variations should have produced corresponding variations of the plume SSS, they are not observed either in Figures 5a, c or at larger temporal lags (not shown). This indirectly indicates that interannual SSS of high variable plume area is not adequately resolved by either of the two profile analyses. Interestingly, both analyses suggest an SSS freshening northeast of the Lesser Antilles (Figures 5a, c) in response to northward shift of the ITCZ, a feature that will be discussed later.

In response to positive (El Nino) phase of the second rainfall mode, which corresponds to depressed rainfall in the tropical Atlantic and Amazon basin (Figure 1b), the open ocean SSS increases by ~0.2 psu/$PC_{unit}$ in a zonally elongated pattern located just north of the equator, which is spatially collocated with the second rainfall mode (Figures 5b, d and Figure 1b). Again, higher plume SSS (otherwise expected due to decreased Amazon discharge, Figure 2d) is not present either in Figures 5 b,d or at larger lags (not shown).

**Satellite SSS** During the AQUARIUS satellite period (SEP2011-MAY2015), the two rainfall modes had a complex behavior including a mission-long trend-like change. The meridional rainfall mode was shifting towards its negative state (Figure 1c) associated with a southward shift of the ITCZ. This shift is forced by the SST-induced meridional gradient of atmospheric pressure and is also reflected in the negative AMM tendency (Figure 6c). Southward shift of the ITCZ enhances rain over the lower Amazon River (Figure 3a) and leads to a quasi-instantaneous increase in its discharge (Figure 2c). This effect was opposed by decreasing tendency in ENSO-induced rainfall (Figure 1c) in response to the warming of equatorial Pacific during its shift from the 2010 La Nina to the 2015 El Nino (Figure 6c). Such shift decreases the Amazon discharge (Figure 2d) due to Pacific SST-induced modification of the Walker Cell. However, during the AQUARIUS period, the impacts of Pacific and Atlantic SSTs compensated each, an effect opposite to the rainfall reinforcement discussed by Ronchail et al. (2002). Despite the Pacific Ocean shift towards El Nino state, the opposite effect associated with the southward shift of the ITCZ slightly dominated over. As a result, the Amazon discharge modestly increased during the AQUARIUS period (not shown).

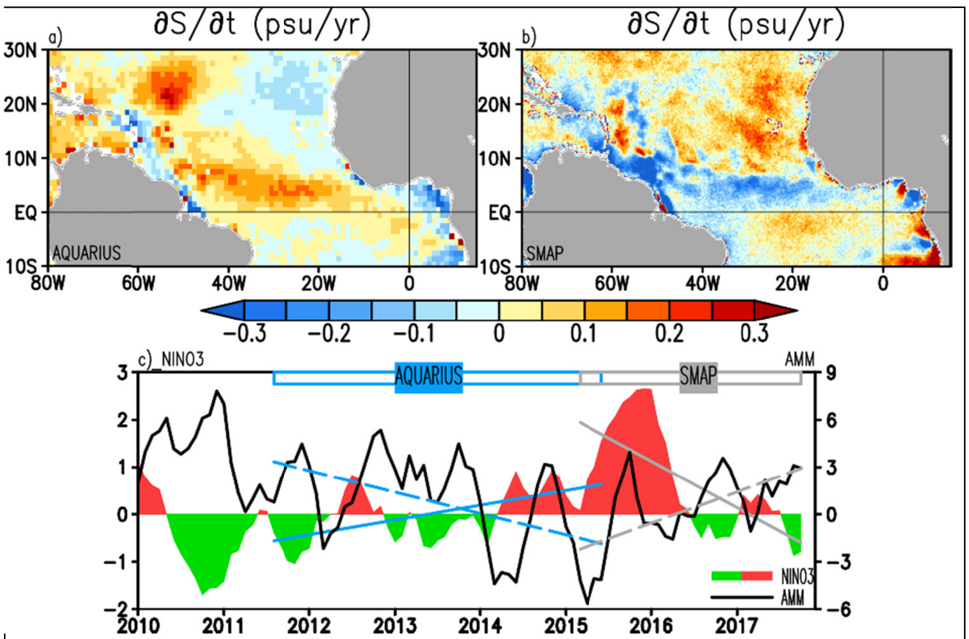


**Figure 6**. Linear temporal slope ($\partial S/\partial t$, psu/year) of (a) AQUARIUS, (b) SMAP anomalous SSS over respective periods of each mission. (c) Time series of NINO3 and Atlantic Meridional Mode (AMM) indices. Linear temporal slope of NINO3 (solid) and AMM (dashed) for AQUARIUS (light blue) and SMAP (gray) period

Noting the presence of trend-like changes in Atlantic rainfall, the AQUARIUS mission long gross change in the surface salinity is characterized next by a linear temporal tendency of de-seasoned SSS (Figure 6a). This reveals a cross-basin tropical Atlantic salinification pattern located just north of the equator (~0.15 psu/year or ~0.6 psu mission long) that reflects the combined effect of increasing Pacific SST and cooling north tropical Atlantic SST. But, the expected freshening corresponding to the south pole of the meridional rainfall mode (Figure 1a) is not present during this particular period. A minor freshening along the northwestern shelf of South America may be attributed to the above mentioned modest increase of Amazon discharge. A salinification tendency northeast of the Lesser Antilles (Figure 6a) may be attributed to changes in the wind-driven ocean circulation in response to strengthening off-shore winds (Figure 1a). Based on Molleri et al. (2010) hypothesis, Fournier et al. (2017) have demonstrated that strengthening northeasterly trades (coincident with anomalous cooling of SST in the north tropical Atlantic and southward shift of the ITCZ) significantly contract the spatial dispersion of the Amazon/Orinoco plume by suppressing the export pathway that delivers fresh water into the north subtropical Atlantic northeast of the Lesser Antilles, and *vice versa*. Missing Amazon fresh water in this area results in apparent contraction of the plume and corresponding up to 0.8 psu (mission long) salinification in the 60W-50W, 20N-30N sector (Figure 6a).

Among interesting features present in Figure 6a (but not well understood yet) is a freshening of the northeastern subtropical Atlantic. Like the Lesser Antilles salt feature, this fresh subtropical feature can be also attributed to an acceleration of northeasterly trade winds, which during the AQUARIUS mission occurred in a pattern corresponding to the negative phase of EOF1 (Figure 1a). On the southeastern periphery of the north subtropical salinity maximum, the anomalously strong northwestward Ekman transport associated with enhanced northeasterly trade winds shrinks the SSS maximum area and thus decreases local salinity.

During the successor, SMAP salinity mission (since late March 2015-onward), the major SST tendencies in the tropical Pacific and Atlantic have been reversing in comparison to the earlier

AQUARIUS period (Figure 6c). Probably, this transition in tendencies reflects the long term AMM variation supported by the wind-evaporation-SST feedback (e.g. Xie and Carton, 2004). As a consequence of this reversal, the low latitude cross Atlantic salinification tendency present during the AQUARIUS period (Figure 6a) has been replaced by a corresponding SSS freshening tendency during the SMAP period (Figure 6b). The latter freshening tendency depicts the ocean response to increasing ENSO-induced Atlantic rainfall during the recent cooling of Pacific SST. Amazon plume SSS also freshened during the SMAP period (Figure 6b) as a result of the Amazon discharge increase after the 2015 El Nino drought.

**Ocean reanalysis salinity** Because temporal variability of SSS in the plume is not completely represented by profile analyses, an ocean data reanalysis, which combines observations with model physics forced by observed variations of the Amazon discharge, is explored. As a proxy for the SSS, the shallowest level (~5m) salinity from the SODA3.4.2 (driven by ERA-I atmospheric fluxes, also used above for the EOF analysis in Figure 1) is employed. As expected, the northward shift of the ITCZ produces a quasi-instantaneous SSS response in the open ocean that resembles observation-based SSS response, is statistically significant and spatially coherent with rainfall EOF1 (compare Figure 7a with Figures 5a,c). In addition to correlation patterns present in observations, SODA-based correlations also show a higher plume salinity, which is expected in response to weaker Amazon discharge during northward excursions of the ITCZ. While the SSS pattern associated with the open ocean rainfall is stronger at small lags and gradually disappears in time (almost vanishes in 8 months after the spring peak of meridional rainfall, Figures 7a,b,c,d), the anomalous salty plume persists and reaches maximal areal extent at 8 month lag (Figure 7c). This persistence time is determined by the annual life span of the

Amazon plume that is limited by the seasonal acceleration of winds in coming boreal winter. Until this seasonal wind strengthening, the plume expands spatially as a result of advection and eddy dispersal and is preserved from the vertical mixing by barrier layers (e.g. Liu et al., 2009). In that sense, the 8 month lag roughly corresponds to the beginning of winter when enhanced stirring associated with increased winds mixed out the plume (e.g. Grodsky et al., 2014a). Note, that winter persistence barrier restricts potential preconditioning of the next year plume properties.

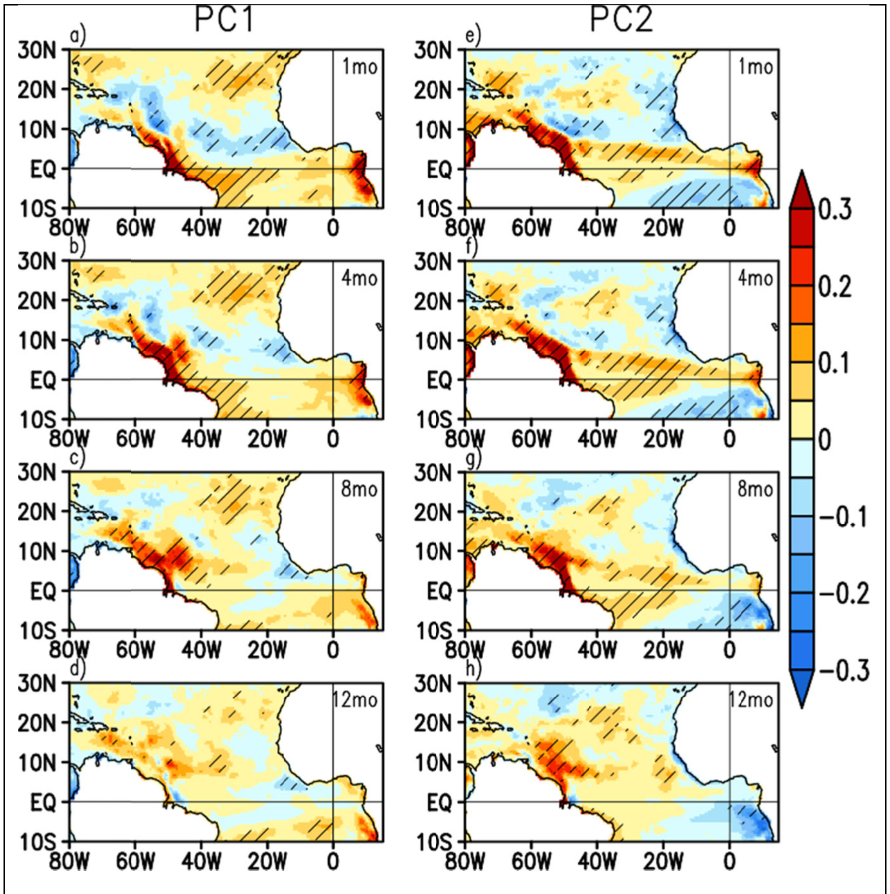


**Figure 7**. Lagged regression of ocean rainfall principal components (from Figure 1c) & monthly anomalous SSS from SODA ocean reanalysis. Color scale is in (psu/$PC_{unit}$). Areas where lagged correlation exceeds the 99% confidence level of zero correlation are hatched.

During El Nino/La Nina, the ENSO-induced rainfall produces a low latitude cross Atlantic salty/fresh pattern, respectively. This pattern is also present in profile observations (Figures 5b,d), AQUARIUS and SMAP satellite data (Figures 6a,b), as well as SODA (Figure 7e). In distinction from observations, the ENSO-induced SSS pattern extends south of the equator in SODA (Figures 7e,f,g). While the pattern located north of the equator collocates with fresh SSS and is linked to variations in local rainfall, the pattern located to the south of the equator collocates with a near-equatorial SSS maximum (Figure 8). From the north, this SSS maximum is bounded by fresh waters diluted by ITCZ rainfall. From the south, it is bounded by relatively fresh SSS, which origin may be linked either to the dynamical effect of a beta-plume evolving from the Congo river plume (Palma and Matano, 2017) or to the seasonal rainfall in the Southern ITCZ (Grodsky and Carton, 2003). Southern pattern collocation with the area of near-equatorial SSS maximum allows hypothesizing that it is generated by ENSO-induced anomalous equatorial easterly winds (Figure 1b) that entrain salty water of the Equatorial Undercurrent (EUC) into the mixed layer (e.g. Grodsky et al., 2006).

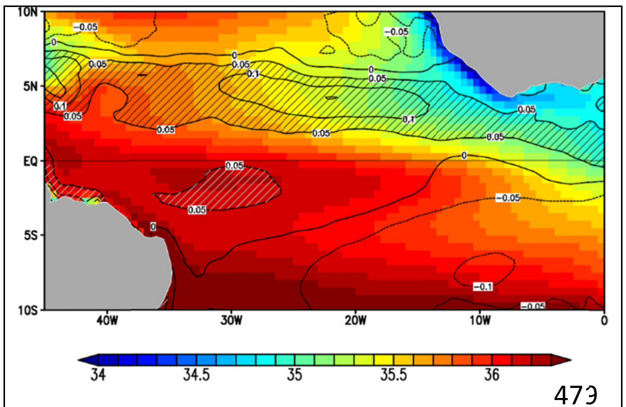


**Figure 8**. Annual mean SODA surface salinity (psu) with ENSO-induced regression pattern from Figure 7e overlain (contours). Regression areas >0.05psu/$PC_{unit}$ are hatched.

The temporal width of lag correlation between NINO3 and PC2 time series ± 6 months (Figure 3b) reflects rather long annual duration of ENSO-induced rainfall that is a consequence of a wide spectrum of atmospheric mechanisms involved in Pacific SST teleconnections (Ronchail et al., 2002). This long duration explains why the cross Atlantic SSS pattern persists at least one season following the peak of ENSO-induced ocean rainfall and still is present at 4 month lag and identifiable at 8 month lag (Figures 7 f,g).

Although the strongest negative correlation between Atlantic rainfall PC2 and Amazon discharge lags behind the rainfall by 3 to 7 months (uncertainty in lag is due to the correlation extremum shape that is rather flat) and occurs roughly during the seasonal maximum of Amazon discharge following behind the late autumn peak of ENSO (Figure 3d), SODA simulations suggest that plume response is already present just in 1 month after the peak of Atlantic rainfall (Figure 7e) when the lagged correlation is only marginally important. The plume response is present at all lags shown in Figure 6 and is still detectable at 12 month lag (Figure 7h). Note, that meridional rainfall response SSS pattern is almost diffused at this lag (Figure 7d). This difference doesn't imply a longer persistence of ENSO-induced anomalous SSS, but simply reflects SSS response to already delayed response of the Amazon discharge (Figure 3d). Like the 8 month lag versus the meridional mode-induced rainfall (that peaks in spring), the 12 month lag versus the ENSO-induced rainfall (ENSO peaks in late autumn through winter) corresponds to the next winter persistence barrier associated with the impact of seasonal wind acceleration over the Amazon plume area.

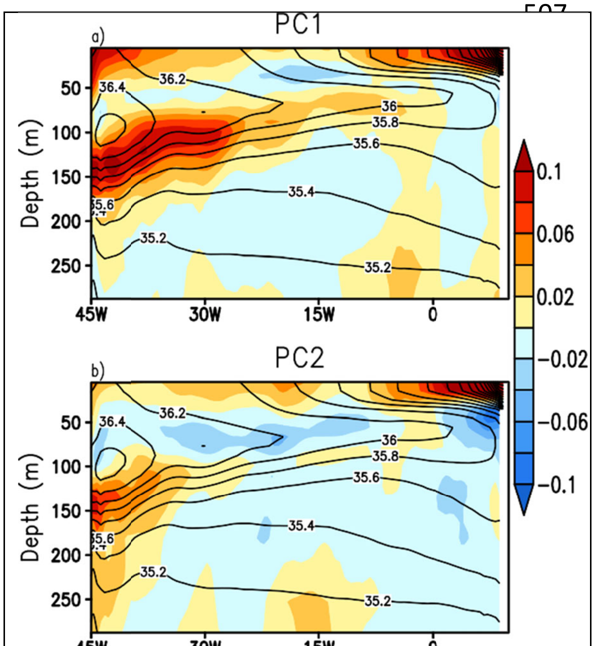


**Figure 9**. Temporal regression of SODA equatorial anomalous salinity ($psu/PC_{unit}$) with (a) meridional rainfall PC1, (b) ENSO rainfall PC2. Rainfall leads salinity by 1 month. Contours are time mean salinity.

The vertical structure of salinity perturbations along the equator combines the surface and wind-driven responses (Figure 9). Surface pattern of anomalous salinity extends down to about 30m. Below, the anomalous salinity is mostly governed by the stationary wind-driven response for which anomalous equatorial zonal wind stress is balanced by anomalous zonal pressure gradient associated with anomalous zonal slope of the thermocline. In response to strengthening of equatorial easterly winds, the thermocline slope increases that is accompanied by its deepening in the west and salinity increase below the EUC salinity maximum. Accompanying modest freshening above the EUC core is also present. This stationary wind response is better seen for the meridional mode PC1 (Figure 9a), for which wind anomalies are stronger than those for the ENSO mode (Figure 1). ENSO-induced salinity response is similar but weaker (Figure 9b) in line with relatively weaker wind perturbations (Figure 1b). Note, that regression patterns in Figure 9 emphasize the stationary response to enhanced zonal winds in the western equatorial Atlantic. Transition processes accompanying individual event adjustment involve the Kelvin-Rossby wave trains discussed e.g. by Foltz et al. (2012) in connection with the 2009 meridional event.

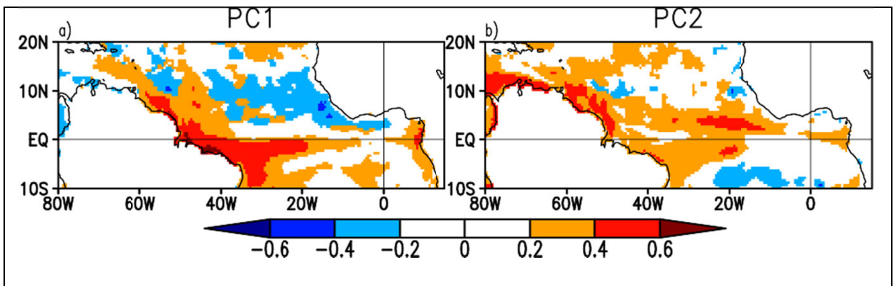


**Figure 10**. Lagged correlation of anomalous SSS with meridional (PC1) and ENSO (PC2) rainfall mode shown at the temporal lag ($-12 < \tau < 12$) corresponding to maximum absolute value of lagged correlation, $\max(|LAGCOR\ (\tau)|)$.

The amplitude of anomalous plume salinity associated with rainfall-induced Amazon discharge is rather weak (~0.3 psu, Figure 7) in comparison to the amplitude of anomalous SSS observed by satellites (~1 psu, Figure 4c). Similar SSS amplitudes have been found by Tyaquiçã et al. (2017, note the scaling of EOF and PC in their Figure 4). The relatively weak magnitude of rainfall/discharge-induced salinity coexists with stronger salinity variations caused by transient processes, with eddy-ocean dynamics contributing among others (e.g. Grodsky et al., 2014a). Intense transient processes lead to only modest correlation of plume SSS with anomalous rainfall (Figure 10). This probably explain why discharge-induced SSS variability in the plume is not resolved well by analyses based on randomly sampled in-situ profiles.

## 4. Summary

Because spatial patterns of interannual rainfall are almost equally partitioned between ocean and land, such partitioning results in a complex SSS response. While SSS response to ocean rainfall is almost instantaneous, its response to land rainfall is delayed by the river hydrology. Such delay is stronger for ENSO-induced rainfall that affects a vast portion of the Amazon drainage area. Resulting Amazon discharge variation lags behind the NINO3 by 3 to 7 months and is accounted for by the volume transport at Obidos. In contrast, the meridional rainfall mode occupies only the lower Amazon drainage area of near coastal northeastern South America. As a result, meridional mode induced variations of the Amazon discharge have a minor (~1 month) delay behind the peak of rainfall, but are not totally accounted for by Obidos transport and require contributions from the major southern tributaries and the Tocantins River.

Temporal regression of anomalous SSS with the two leading principal components of anomalous rainfall is consistent for the JAMSTEC and SCRIPPS in-situ profile analyses and depicts an expected surface-forced SSS response that maximizes quasi-instantaneously with rainfall (a minor few month lag is present) and closely corresponds to its spatial patterns. During positive phases of the meridional (dipole) rainfall mode (corresponding to northward shifts of the ITCZ), the SSS decreases in the 5N-10N corridor and increases off the eastern tip of South America. The magnitude of SSS anomaly ~0.15 psu/$PC_{unit}$ suggests up to 0.5 psu interannual variation. ENSO-induced rainfall is represented by the second mode that describes in-phase variations of tropical Atlantic rainfall in spatially coherent zonally elongated pattern crossing the basin.

During El Nino, the anomalous surface freshwater forcing associated with depressed tropical Atlantic rainfall increases local SSS by ~0.2 psu/$PC_{unit}$.

Although both rainfall modes imprint on anomalous Amazon discharge, the effect of varying discharge on the plume SSS is not present in either of in-situ profile analyses. The latter is better represented by SODA3 ocean reanalysis due to embedded physics forced by observed variations of the Amazon discharge. SODA reveals that Amazon plume SSS anomalies are present during 8 months following the meridional mode rainfall peak and during almost 1 year after the ENSO mode rainfall peak. Longer persistence of ENSO-induced plume SSS is explained by the memory associated with the Amazon hydrology and the corresponding delay of the Amazon discharge behind the rainfall. The magnitude of consistent response of plume SSS evaluated from temporal regression with time series of principal components of the ocean rainfall modes is a modest few tenth of PSU and only marginally statistically important. Perhaps, such relatively weak correlation is not surprising given a variety of other factors contributing in this dynamically active area. It may also explain why profile analyses, which are based on random in-situ casts, don't sample well temporal variability of the plume properties.

During the satellite SSS epoch, the two rainfall modes had a complex behavior, including mission-long trend-like changes. During the earlier AQUARIUS period (SEP2011-MAY2015), the ITCZ was shifting southward. This ITCZ shift resulted in a corresponding enhancement of rainfall over the lower Amazon River. Concurrently, the effect of warming eastern equatorial Pacific SST forced a decrease of ENSO-induced rainfall in the Atlantic sector. Compensating impacts of Pacific and Atlantic SSTs resulted in rather stable Amazon discharge with weak increase dominated by the meridional rainfall mode. As a result of these compensating changes, the AQUARIUS mission long anomalous SSS tendency is concentrated in the cross-basin tropical Atlantic salinification pattern located just north of the equator (~0.15 psu/year or ~0.6 psu mission long) that reflects the combined, in phase effect of increasing Pacific SST and cooling north tropical Atlantic SST on the open ocean rainfall. During the successor, SMAP salinity mission (since late March 2015-onward), the major SST tendencies in the tropical Pacific and Atlantic have been reversing in comparison to the AQUARIUS period. As a consequence of this reversal, the low latitude cross Atlantic salinification tendency present in the AQUARIUS SSS has been replaced by a freshening tendency in the SMAP SSS, which depicts the open ocean response to increasing ENSO-induced Atlantic rainfall during the recent cooling of Pacific SST. In distinction from the AQUARIUS period when the Amazon plume didn't show any noticeable SSS trend, the later SMAP period includes a freshening tendency in the plume in response to the increase of Amazon discharge after the 2015 El Nino drought.

**Acknowledgements** Supported by NASA/OSST. This research is based on various data that are freely distributed and listed in the Data section.

## 5. References

Adler, R. F., G. J. Huffman, A. Chang, R. Ferraro, P. Xie, J. Janowiak, B. Rudolf, U. Schneider, S. Curtis, D. Bolvin, A. Gruber, J. Susskind, P. Arkin, and E. Nelkin, 2003: The version 2 Global Precipitation Climatology Project (GPCP) monthly precipitation analysis (1979-present). *J. Hydrometeor*, 4(6), 1147-1167.

Amarasekera, K. N., R. F. Lee, E. R. Williams, and E. Eltahir (1997), ENSO and the natural variability in the flow of tropical rivers. *J. Hydrol.*, **200**(1–4), 24–39. http://dx.doi.org/10.1016/S0022-1694(96)03340-9

Carton, J.A., and E.J. Katz (1990), Estimates of the zonal slope and seasonal transport of the Atlantic North Equatorial Countercurrent, *J. Geophys. Res*., **95**, 3091-3100, DOI: 10.1029/JC095iC03p03091.

Chen, J. L., C. R. Wilson, and B.D. Tapley (2010). The 2009 exceptional Amazon flood and interannual terrestrial water storage change observed by GRACE. *Water Resources Research*, *46*(12), W12526. http://dx.doi.org/10.1029/2010WR009383

Chiang, J. C. H., Y. Kushnir, and A. Giannini (2002), Deconstructing Atlantic Intertropical Convergence Zone variability : Influence of the local cross-equatorial sea surface temperature gradient and remote forcing from the eastern equatorial Pacific, *J. Geophys. Res.*, *107*(D1), 4004. https://doi.org/10.1029/2000JD000307

Chiang, J. C. H. and D. J. Vimont (2004), Analagous meridional modes of atmosphere-ocean variability in the tropical Pacific and tropical Atlantic. *J. Climate, 17* (21), 4143–4158.

Dai, A., T. Qian, K. E. Trenberth, and J. D. Milliman (2009), Changes in continental freshwater discharge from 1948 to 2004. *J. Clim.*, *22*, 2773–2792, doi:10.1175/2008JCLI2592.1.

Dai, A. (2016), Historical and Future Changes in Streamflow and Continental Runoff: A Review, In *Terrestrial Water Cycle and Climate Change: Natural and Human-Induced Impacts* (pp. 17–37). https://doi.org/10.1002/9781118971772.ch2

Dee, D.P., Uppala, S.M., Simmons, A.J., Berrisford, P., Poli, P., Kobayashi, S., Andrae, U., Balmaseda, M.A., Balsamo, G., Bauer, P., Bechtold, P., Beljaars, A.C.M., van de Berg, L., Bidlot, J., Bormann, N., Delsol, C., Dragani, R., Fuentes, M., Geer, A.J., Haimberger, L., Healy, S.B., Hersbach, H., Holm, E.V., Isaksen, L., Kallberg, P., Kohler, M., Matricardi, M., AP, McNally, Monge-Sanz, B.M., Morcrette, J.-J., Park, B.- K., Peubey, C., de Rosnay, P., Tavolato, C., Thepaut, J.-N., Vitart, F. (2011), The ERAInterim reanalysis: configuration and performance of the data assimilation system. *Q. J. R. Meteorol. Soc. 137*, 553–597. http://dx.doi.org/10.1002/qj.828.

Dessier, A., and J.R. Donguy (1994), The sea surface salinity in the tropical Atlantic between 10°S and 30°N – seasonal and interannual variations (1977-1989), *Deep Sea Res. I*, *41*, 81-100, http://dx.doi.org/10.1016/0967-0637(94)90027-2 .

Enfield, D. B., and D. A. Mayer (1997), Tropical Atlantic sea surface temperature variability and its relation to El Niño-Southern Oscillation, *J. Geophys. Res. Ocean.*, *102*(C1), 929–945. https://doi.org/10.1029/96JC03296

Espinoza, J. C., J. Ronchail, J.L. Guyot, G. Cochonneau, N. Filizola, W. Lavado, E. de Oliveira, R. Pombosa, and P. Vauchel (2009), Spatio – Temporal rainfall variability in the Amazon Basin Countries (Brazil, Peru, Bolivia, Colombia and Ecuador). *International Journal of Climatology, 29*, 1574-1594. http://dx.doi.org/10.1002/JOC.1791

Espinoza, J. C., H. Segura, J. Ronchail, G. Drapeau, and O. Gutierrez-Cori (2016), Evolution of wet-day and dry-day frequency in the western Amazon basin: Relationship with atmospheric circulation and impacts on vegetation, *Water Resour. Res., 52*, 8546–8560, doi:10.1002/2016WR019305.

Gill, A. E. (1980), Some simple solutions for heat-induced tropical circulation. *Q.J.R. Meteorol. Soc.*, *106*, 447–462. doi:10.1002/qj.49710644905.

Grodsky, S.A. and J.A. Carton (2003), The Intertropical Convergence Zone in the South Atlantic and the Equatorial Cold Tongue. *J. Climate, 16*, 723–733, https://doi.org/10.1175/1520-0442(2003)016<0723:TICZIT>2.0.CO;2

Grodsky, S. A., J. A. Carton, and F. M. Bingham (2006), Low frequency variation of sea surface salinity in the tropical Atlantic, *Geophys. Res. Lett.*, *33*(14). https://doi.org/10.1029/2006GL026426

Grodsky, S. A., N. Reul, G. S. E. Lagerloef, G. Reverdin, J. A. Carton, B. Chapron, Y. Quilfen, V. N. Kudryavtsev, and H.-Y. Kao (2012), Haline hurricane wake in the Amazon/Orinoco plume: AQUARIUS/SACD and SMOS observations, *Geophys. Res. Lett.*, *39*, L20603, doi:10.1029/2012GL053335.

Grodsky, S.A., G. Reverdin, J. A. Carton, and V. J. Coles (2014a), Year-to-year salinity changes in the Amazon plume: Contrasting 2011 and 2012 Aquarius/SACD and SMOS satellite data, *Remote Sensing of Environment*, *140*, 14-22, http://dx.doi.org/10.1016/j.rse.2013.08.033.

Grodsky, S. A., J. A. Carton, and F. O. Bryan (2014b), A curious local surface salinity maximum in the northwestern tropical Atlantic, *J. Geophys. Res. Oceans, 119*, 484–495, doi:10.1002/2013JC009450.

Hastenrath, S., and L. Heller (1977), Dynamics of climatic hazards in northeast Brazil, *Q. J. R. Meteorol. Soc.*, *103*(435), 77–92. https://doi.org/10.1002/qj.49710343505

Hosoda, S., T. Ohira, and T. Nakamura (2008), A monthly mean dataset of global oceanic temperature and salinity derived from Argo float observations, *JAMSTEC Rep. Res. Dev.*, 8, 47-59, available online at http://www.argo.ucsd.edu/Hosoda_etal_MOAA_GPV.pdf

Foltz, G. R., S. A. Grodsky, J. A. Carton, and M. J. McPhaden (2004), Seasonal salt budget of the northwestern tropical Atlantic Ocean along 38°W, *J. Geophys. Res*., *109,* C03052, doi:10.1029/2003JC002111.

Foltz, G.R., M.J. McPhaden, and R. Lumpkin (2012), A Strong Atlantic Meridional Mode Event in 2009: The Role of Mixed Layer Dynamics. *J. Climate,* **25**, 363–380, https://doi.org/10.1175/JCLI-D-11-00150.1

Foltz, G.R., C. Schmid, and R. Lumpkin (2015), Transport of surface freshwater from the equatorial to the subtropical North Atlantic Ocean. *J. Phys. Oceanogr.*, *45*, 1086-1102, doi:10.1175/JPO-D-14-0189.1.

Fournier, S., D. Vandemark, L. Gaultier, T. Lee, B. Jonsson, and M.M. Gierach (2017). Interannual variation in offshore advection of Amazon-Orinoco plume waters: observations, forcing mechanisms, and impacts. *Journal of Geophysical Research Oceans*, DOI 10.1002/2017JC013103

Kousky, V. E., M. T. Kagano, and I. F. A. Cavalcanti (1984), A review of the Southern Oscillation: oceanic-atmospheric circulation changes and related rainfall anomalies, *Tellus A*, *36 A*(5), 490–504. https://doi.org/10.1111/j.1600-0870.1984.tb00264.x

Lee, T. (2016), Consistency of Aquarius sea surface salinity with Argo products on various spatial and temporal scales, *Geophys. Res. Lett., 43*, 3857–3864, doi:10.1002/2016GL068822.

Lentz, S. J. (1995). Seasonal variations in the horizontal structure of the Amazon Plume inferred from historical hydrographic data, *Journal of Geophysical Research*, *100*(C2), 2391–2400. http://dx.doi.org/10.1029/94JC01847 .

Liu, H., S.A. Grodsky, and J.A. Carton (2009), Observed subseasonal variability of oceanic barrier and compensated layers, *J. Climate: 22*, 6104-6119, DOI: 10.1175/2009JCLI2974.1.

Meissner.T, and F. Wentz (2016), RSS SMAP Salinity: Version 2 Validated Release, RSS Technical Report 091316, Remote Sensing Systems, Santa Rosa, CA, 23 pp. (available online at [ftp://ftp.remss.com/smap/SSS/Release_V2.0.pdf](ftp://ftp.remss.com/smap/SSS/Release_V2.0.pdf) )

Molleri, G.S.F., E.M.L. de M. Novo, and M. Kampel (2010), Space-time variability of the Amazon River plume based on satellite ocean color, *Continental Shelf Research, 30*, 342-352, http://dx.doi.org/10.1016/j.csr.2009.11.015.

Nobre, P., and J. Shukla (1996), Variations of Sea Surface Temperature, Wind Stress, and Rainfall over the Tropical Atlantic and South America. *J. Climate, 9*, 2464–2479, https://doi.org/10.1175/1520-0442(1996)009<2464:VOSSTW>2.0.CO;2

Palma, E. D., and R. P. Matano (2017), An idealized study of near equatorial river plumes, *J. Geophys. Res. Oceans, 122*, 3599–3620, doi:10.1002/2016JC012554.

Roemmich, D., and J. Gilson (2009), The 2004–2008 mean and annual cycle of temperature, salinity, and steric height in the global ocean from the Argo Program, *Progress in Oceanography*, *82*(2), 81-100, https://doi.org/10.1016/j.pocean.2009.03.004 .

Ronchail, J., G. Cochonneau, M. Molinier, J.-L. Guyot, A. G. De Miranda Chaves, V. Guimarães, and E. de Oliveira (2002), Interannual rainfall variability in the Amazon basin and sea-surface temperatures in the equatorial Pacific and the tropical Atlantic Oceans, *Int. J. Climatol.*, *22*(13), 1663–1686. https://doi.org/10.1002/joc.815

Ropelewski, C.F. and M.S. Halpert, 1987: Global and Regional Scale Precipitation Patterns Associated with the El Niño/Southern Oscillation. *Mon. Wea. Rev., 115*, 1606–1626, https://doi.org/10.1175/1520-0493(1987)115<1606:GARSPP>2.0.CO;2

Sasaki, W., T. Doi, K.J. Richards, and Y. Masumoto (2015), The influence of ENSO on the equatorial Atlantic precipitation through the Walker circulation in a CGCM, *Clim. Dyn*., *44*(191), doi:10.1007/s00382-014-2133-5

Tyaquiçã, P., D. Veleda, N. Lefèvre, M. Araujo, C. Noriega, G. Caniaux, J. Servain, and T. Silva (2017), Amazon Plume Salinity Response to Ocean Teleconnections, *Front. Mar. Sci.,* *4*(250). doi: 10.3389/fmars.2017.00250

Yoon, J. H., and N. Zeng (2010), An Atlantic influence on Amazon rainfall, *Climate Dynamics*, *34*(2), 249–264. https://doi.org/10.1007/s00382-009-0551-6

Yu, L. (2015), Sea-surface salinity fronts and associated salinity-minimum zones in the tropical ocean, *J. Geophys. Res. Oceans, 120,* 4205–4225*,* doi:10.1002/2015JC010790.

Zeng, N., Yoon, J., Marengo, J., Subramaniam, A., Nobre, C.,Mariotti, A., and J. D. Neelin (2008), Causes and impacts of the 2005 Amazon drought, *Environmental Research Letters,* *3*, 014002. http://dx.doi.org/10.1088/1748-9326/3/1/014002 .

## 6. Figures

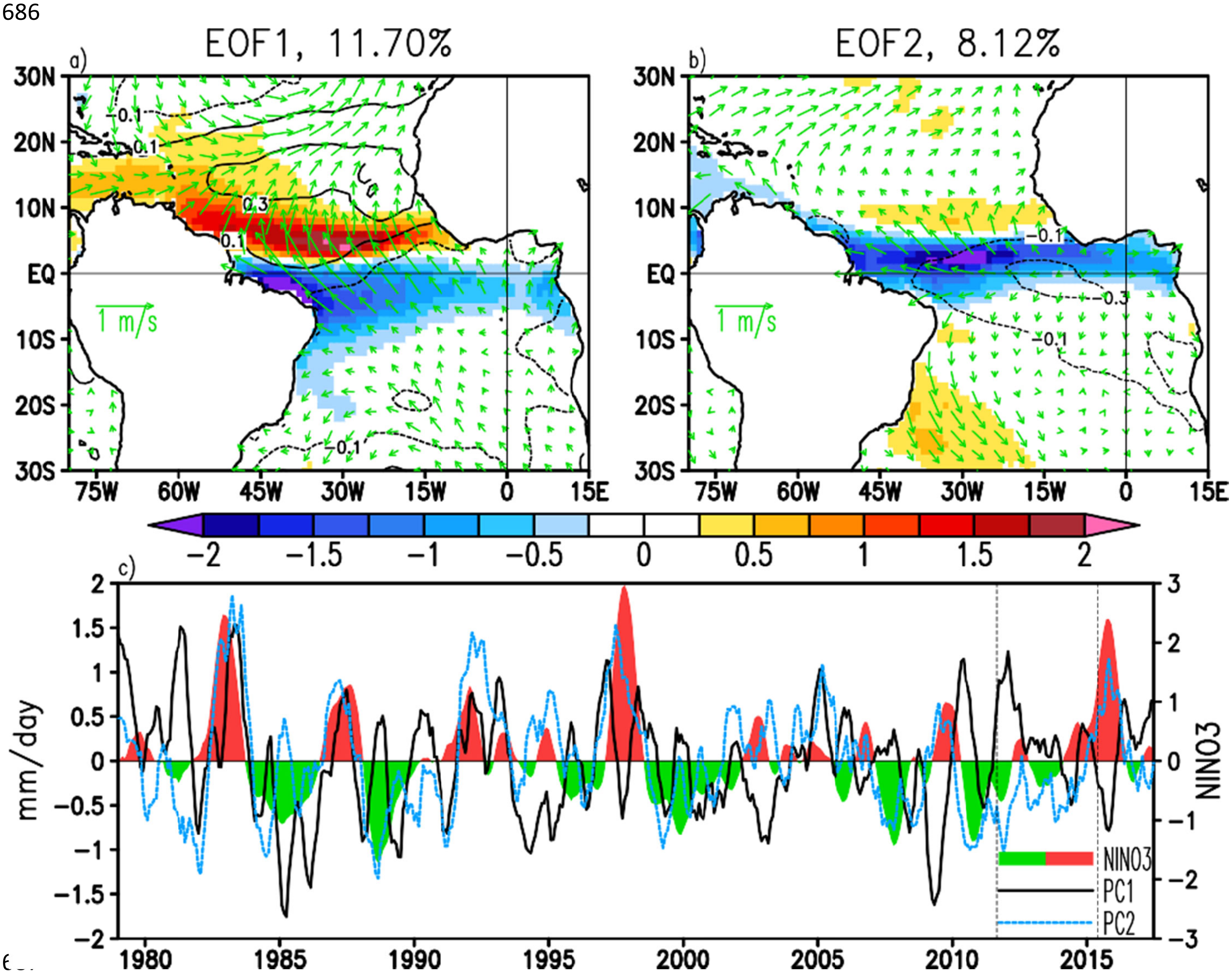


**Figure 1**. (a,b) Spatial (EOF) and (c) temporal (PC) parts of the two leading EOFs of anomalous monthly ERA-I rainfall-minus-evaporation. Corresponding PC regression with anomalous SST (contours, degC) and 10m wind (arrows) are also shown in (a) and (b). NINO3 index is shown in (c). All time series are ±3 month smoothed. Vertical lines in (c) mark the AQUARIUS period.

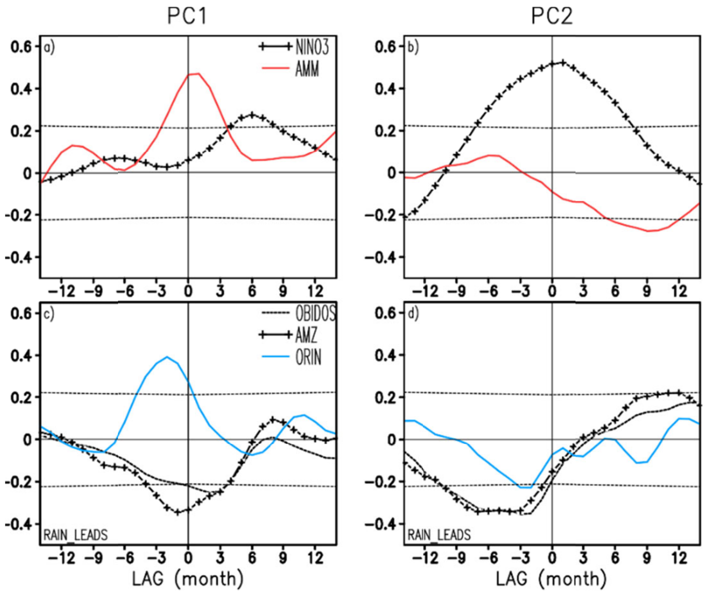


**Figure 2**. Lagged correlation of ocean rainfall principal components (from Figure 1c) with (a, b) NINO3 and Atlantic Meridional Mode (AMM) indices, (c, d) anomalous monthly Amazon volume transport at Obidos station, combined Amazon transport (from Obidos, Xingu, Tapajos, and Tocantins, AMZ), and Orinoco transport (ORIN). The 99% confidence intervals of zero correlation are shown by thin dashed lines.

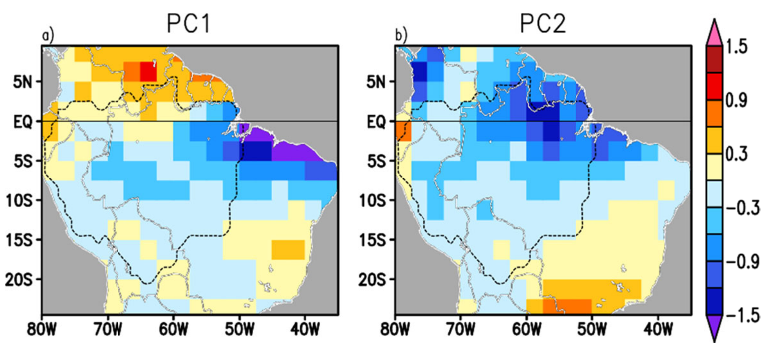


**Figure 3**. Temporal regression of ocean rainfall principal components (Figure 1c) on GPCP land rainfall (mm/dy) for (a) meridional rainfall mode (PC1) and (b) ENSO rainfall mode (PC2). Amazon catchment area is shown by dashed.

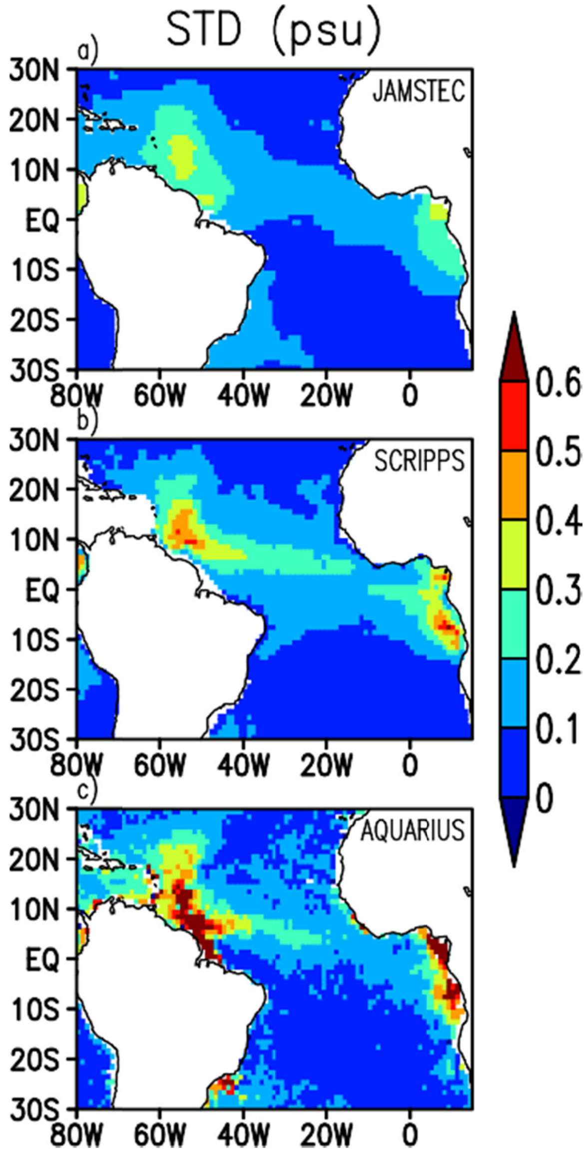


**Figure 4.** Standard deviation (STD) of monthly SSS anomaly from in-situ profile analyses (a) JAMSTEC, (b) SCRIPPS, and (c) AQUARIUS satellite.

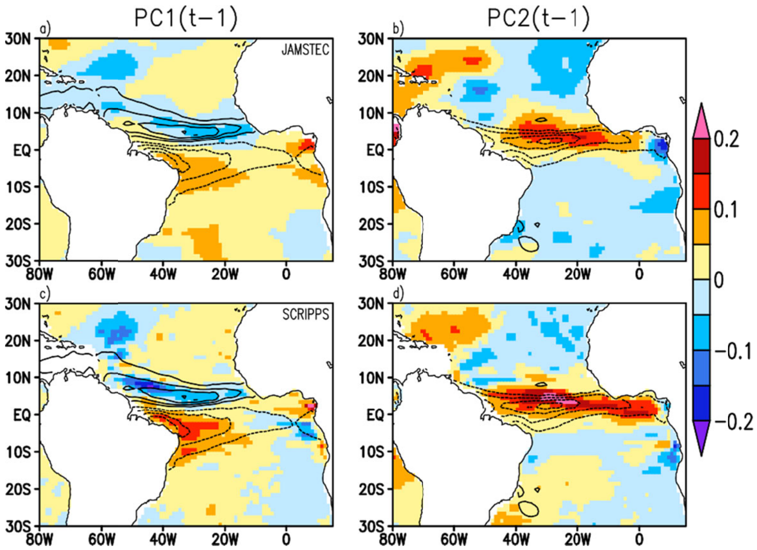


**Figure 5**. Temporal regression of ocean rainfall principal components (from Figure 1c) with monthly anomalous SSS from (a,b) JAMSTEC, (c, d) SCRIPPS. Color scale is in (psu/$PC_{unit}$). Regression maps correspond to PC1 and PC2 leading SSS by 1 month. Spatial rainfall EOFs (Figure 1a, b) are overlain as contours.

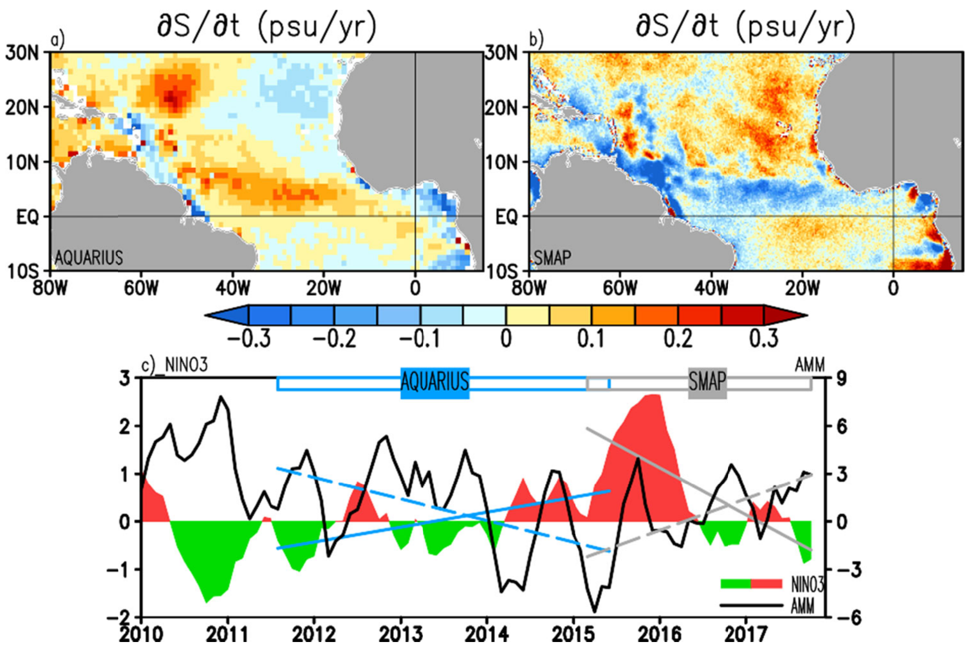


**Figure 6**. Linear temporal slope ($\partial S/\partial t$, psu/year) of (a) AQUARIUS, (b) SMAP anomalous SSS over respective periods of each mission. (c) Timeseries of NINO3 and Atlantic Meridional Mode (AMM) indices. Linear temporal slope of NINO3 (solid) and AMM (dashed) for AQUARIUS (light blue) and SMAP (gray) period.

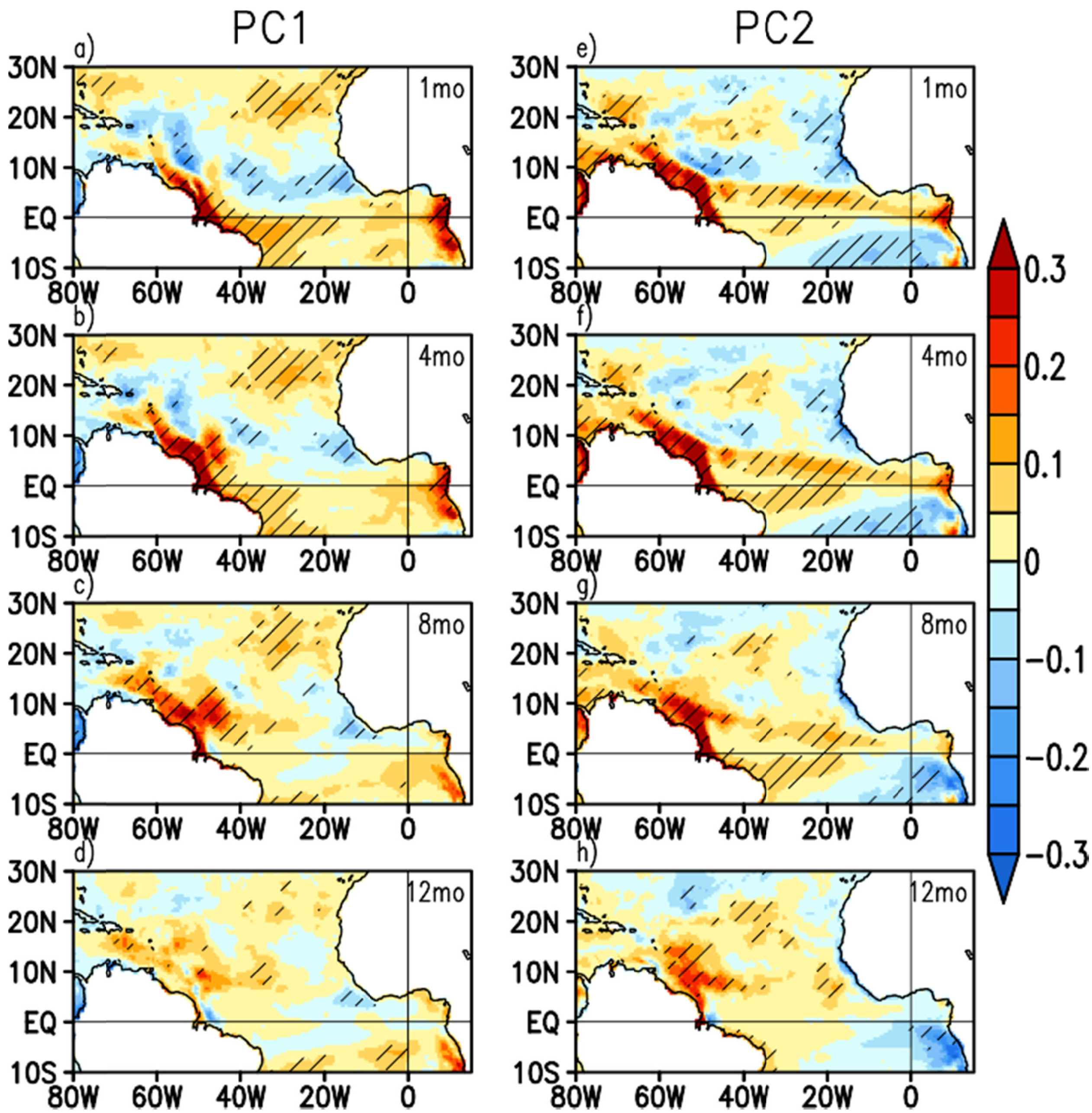


**Figure 7**. Lagged regression of ocean rainfall principal components (from Figure 1c) with monthly anomalous SSS from SODA ocean reanalysis. Colorscale is in ($psu/PC_{unit}$). Areas where lagged correlation exceeds the 99% confidence level of zero correlation are hatched.

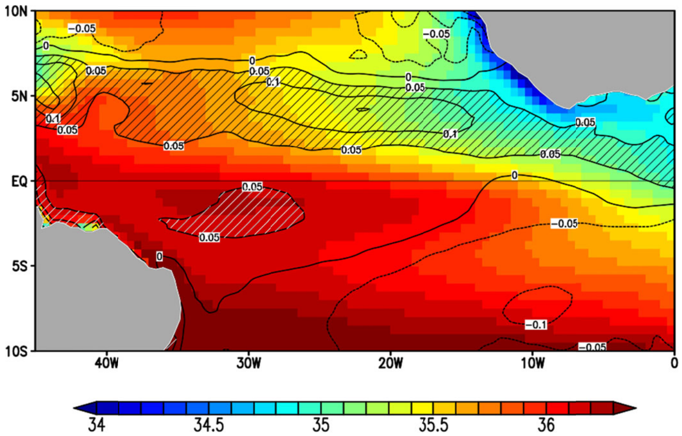


**Figure 8**. Annual mean SODA surface salinity (psu) with ENSO-induced regression pattern from Figure 7e overlain (contours). Regression areas >0.05psu/$PC_{unit}$ are hatched.

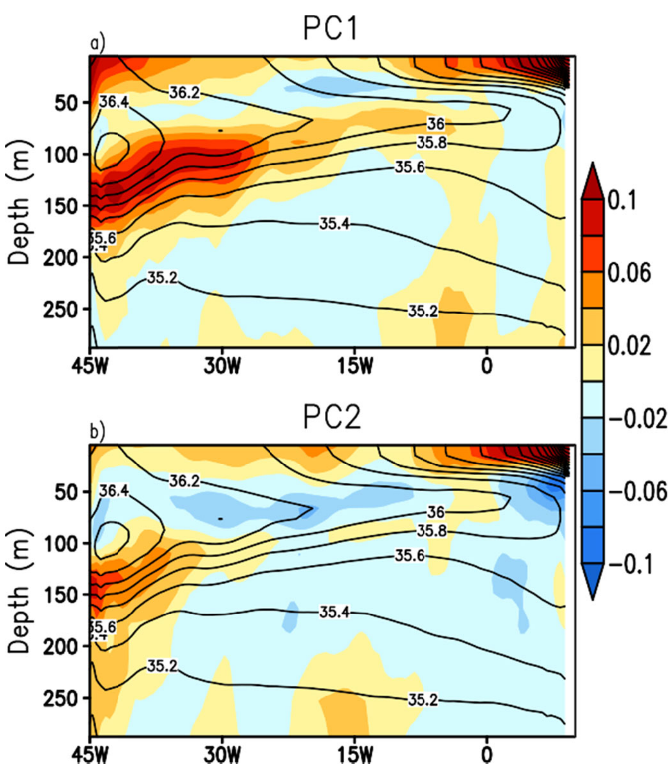


**Figure 9**. Temporal regression of SODA equatorial anomalous salinity (psu/$PC_{unit}$) with (a) meridional rainfall PC1, (b) ENSO rainfall PC2. Rainfall leads salinity by 1 month. Contours are time mean salinity.

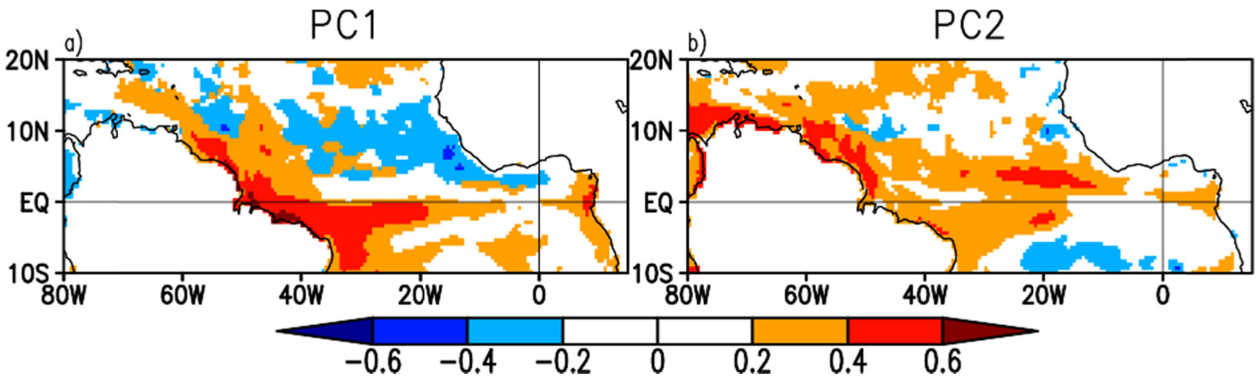


**Figure 10**. Lagged correlation of anomalous SSS with meridional (PC1) and ENSO (PC2) rainfall mode shown at the temporal lag ($-12 < \tau < 12$) corresponding to maximum absolute value of lagged correlation, $\max(|LAGCOR\ (\tau)|)$.

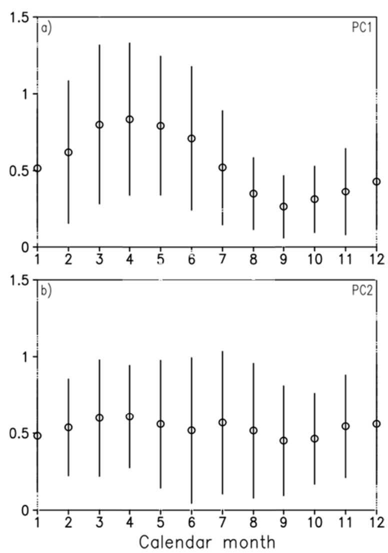


Figure 9. Mean ('o') and standard deviation (bars) of absolute value of rainfall PC, $|PC|$, for each calendar month for (a) meridional, (b) ENSO modes.